



A descriptive study of dust storms and air quality in a semi-arid region of Mexico

María de Jesús Guevara-Macías¹ · Luis F. Pineda-Martínez² · Noel Carbajal¹

Received: 2 February 2023 / Accepted: 20 April 2023 / Published online: 27 April 2023
© The Author(s), under exclusive licence to Springer Nature B.V. 2023

Abstract

Dust storms are a common phenomenon in arid and semi-arid regions of the world. The erosion in the desert, agricultural, urban, and rural areas contributes to atmospheric mineral dust. Low vegetation cover drives intense dust storms in arid regions like northern Mexico and the southwestern USA. The seasonality associated with winter cold fronts from October to June regulates dust storms. The impact of dust storms is considerable, from massive soil deterioration to health problems caused by policies of changing land use from grasslands and forests to rainfed agriculture. This process has increased notably in recent decades. To identify potential dust storm events, we applied the criterion of a threshold wind speed of 9 m/s in all meteorological stations and data from the Cloud-Aerosol Lidar and Infrared Pathfinder Satellite Observations (CALIPSO) satellite. The analysis of wind data allowed identifying 245 cases of potential dust storms occurring between 2006 and 2018, but only 15 were chosen to be analyzed by numerical modeling. The WRF-Chem model version 3.6 was applied. Numerical experiments allowed calculating the fraction of PM₁₀ emitted during each simulated event, where the concentration varied from 34 to 350 $\mu\text{g}/\text{m}^3$. From the CALIPSO profiles, the atmospheric dust from the outputs of the numerical simulations was verified. Extensive distribution of dust revealed high contributions of PM₁₀ that affect the air quality. The analysis of 13 years of wind data yielded 9 extreme wind events each year exceeding the speed threshold for dust removal.

Keywords Dust storms · PM₁₀ · WRF-Chem · CALIPSO

Introduction

The phenomenon of dust storms recurrently happens in arid and semi-arid regions of the world (Dong et al. 2000; Prospero et al. 2002; Joshi 2021). The principal surface sources of atmospheric mineral dust are related to erosion processes in deserts and agricultural areas, including urban and rural areas with many unpaved roads. Global urban expansion has led to severe land use change due to population growth and food demands (Foley et al. 2005). One of the effects of this land use change is the loss of native plant cover due to crop areas, mainly in the tropical and semi-arid regions of the world (Lambin et al. 2003). Some studies describe the environmental conditions that prevail during dust storms

(Rivera-Rivera et al. 2009 and 2010; Lu et al. 2013; Kok et al. 2017; Hyde et al. 2018). Pineda-Martínez et al. (2011) showed how dust storms could significantly contribute to the energy balance by causing a decrease in incident solar radiation. Csavina et al. (2014) revealed that mineral dust in northern Mexico affected air quality in Mexico and the USA. Álvarez and Carbajal (2019) investigated the effect of air quality deterioration, Choi and Fernando (2008) studied the low visibility, and even the impact on the hydrological cycle was a research theme (Zhao et al. 2012). In China, the land use of rangeland zones in semi-arid and arid areas to introduce mixed farming-grazing practices resulted in land degradation caused by wind erosion (Wang et al. 2004). On the Colorado Plateau in the USA, changes in vegetation cover, primarily perennial vegetation, accelerate dust emission rates during severe wind storms (Munson et al. 2011). In southern Iran, arid conditions and harsh winds cause extreme dust storms associated with increased agricultural frontier (Rezaei et al. 2016). Intense winds in arid regions of northern Mexico and the southwestern USA with low vegetation cover generate extensive dust storms (Csavina et al.

✉ Luis F. Pineda-Martínez
lpineda@uaz.edu.mx

¹ Department of Geosciences, Potosi Institute for Scientific and Technological Research AC., San Luis Potosí, Mexico

² Earth Sciences, Autonomous University of Zacatecas, Zacatecas, Mexico

2014; Lu et al. 2013; Hyde et al. 2018; Álvarez & Carbajal 2019; Joshi 2021).

In general terms, dust storms are classified according to their seasonality and the mechanisms associated with their genesis. The first group of dust storms is related to winter cold fronts from October to June. The second group is generated during the summer monsoon from July to September, known as haboobs (Hyde et al. 2018). Both cause environmental problems, such as the deterioration of air quality, respiratory problems, and erosion of the superficial layers in agricultural soils.

Due to its arid conditions, the region of central and northern Mexico, in the Chihuahuan Desert, is a notable area in the world where strong winds, linked with the passage of cold fronts in winter, frequently cause dust storms. However, large territories within the Mexican border have yet to be studied. Consequently, this region has a very low density of meteorological observation stations and only a few monitoring sites for air quality. The lack of information causes ineffective public programs for preventing soil loss, growing desert dune zones, negative impacts on health, and emerging issues such as the immediate effect of severe dust storms in visibility reduction (Karegar et al. 2019). Health effects due to severe dust storms have been documented in different parts of the world. In Australia, the low air quality and the consequent damage to health was dramatically reflected in the emergency cases admitted, which increased significantly by 39% (Barnett et al. 2012). In the USA, Grineski et al. (2011) documented a correlation between dust events and admissions in hospitals for respiratory diseases. Dust storms affect people of all ages. An increase in the frequency and variety of the chemical composition of dust affects the elderly and young people, especially people with chronic cardiopulmonary diseases (Schweitzer et al. 2018). Middleton (2017) reviews the effects of dust storms on people's health. He considers the frequency, intensity, time scales, long-range transport, and dust trajectories induced by seasonality as essential factors, in addition to existing factors such as the growth of areas that become dust sources and complex chemical composition.

The monitoring network of the National Air Quality Information System (SINAICA) in Mexico and the Aerosol Robotic Network (AERONET) (Holben et al. 1998) has a “geographical gap” in the region's sites due to the low density of large urban areas, its inaccessibility, and remote communication systems. In addition to the monitoring sites' high installation and maintenance costs, they are far from large urban centers. Furthermore, the lack of maintenance of the existing stations generates gaps in the time series.

There are currently operational data alternatives to estimate the presence of atmospheric mineral dust through satellite observations (Basha 2015; Hyde et al. 2018; Karegar et al. 2019). Some studies have used observational data from

MODIS (Karegar et al. 2019) and Cloud-Aerosol Lidar and Infrared Pathfinder Satellite Observations (CALIPSO) (Winker et al. 2007; Basha 2015) to determine the occurrence of atmospheric dust where surface information is unavailable. It is essential to consider the geographical distribution to monitor aerosols and air pollutants because fugitive emissions can affect air quality in cities and small urban areas located far from the emission source. For instance, this occurs in the north and northeast of Mexico, such as Monterrey, including cities south of Texas in the USA (Lu et al. 2013; Csavina et al. 2014). The importance of this research consists in supporting the knowledge of dust storm dynamics and their role in air quality degradation in the study region.

Numerical modeling offers an analysis tool for some of the effects of dust storms from a dynamic point of view. It represents the motivation to analyze dust storms in central and northern regions of Mexico by applying the WRF-Chem numerical model and satellite data to determine the presence of atmospheric mineral dust. The main objective is to estimate the effect on soil erosion of the emission of particulate matter (PM) in dust storms generated in agricultural areas of the state of Zacatecas and to analyze the deterioration of air quality by applying numerical modeling and determining the presence of dust in the study region through data from the CALIPSO lidar profiles. The manuscript is organized as follows: the second section describes the model and data set used. In the third section we include a soil analysis of the dust sources, a validation of the model, and we show the main results and the discussion of the simulated storms and their main characteristics. The last section presents the conclusions as well as some of the limitations of the study.

Methods

Dust storm identification

The meteorological dataset was obtained from the network of automatic stations of INIFAP (2018) (available at <http://www.zacatecas.inifap.gob.mx>) and, additionally, from the Zacatecas International Airport (ZCL) (Fig. 1a). Some minimum conditions are required for a dust event to develop and contribute to atmospheric aerosols as a dust storm. The dataset revealed that maximum sustained wind action could trigger dust storms in winter. However, other factors like geomorphology, soil type, texture, soil moisture, and air humidity have been extensively studied (Wang et al. 2008; Liu et al. 2008; Csavina et al. 2014). We used the criterion of a threshold wind speed of 9 m/s due to the lack of information on surface aerosol and atmospheric particulate matter concentrations to identify potential dust storm events. This research considers a threshold speed of 9 m/s even for cases with RH above

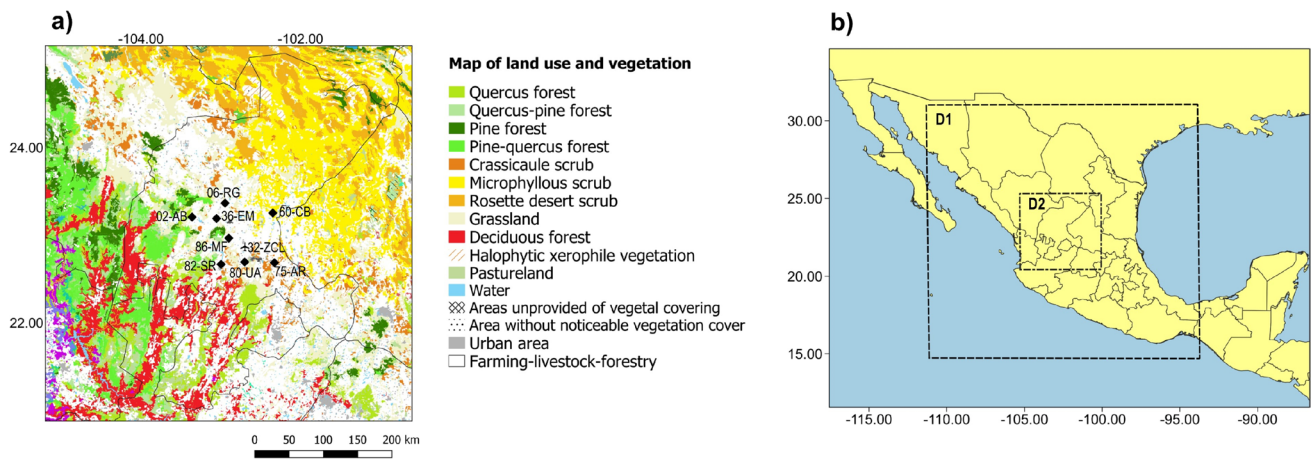


Fig. 1 a Land use and vegetation map (modified from INEGI 2015); dots indicate the localization of weather stations: Ábrego 02-AB, Emancipación 36-EM, Mesa de Fuentes 86-MF, 06-Rancho Grande RG, Santa Rita 82-SR, Agronomía 80-UA, Las Arcinas 75-AR,

COBAEZ 60-CB, and Zacatecas International Airport 32-ZCL, and b location map of the study area, dotted lines indicate the simulated area in WRF-Chem domain one (D1) and domain two (D2)

50%. This threshold is higher than the values suggested by Csavina et al. (2014), where they identified an increase in the concentration of TSP and PM₁₀ with speeds above 4 m/s and 5 m/s, considering a relative humidity < 40% as an additional factor. From a detailed analysis of the wind speed data for all meteorological stations from October 2005 to April 2018, we examined the events where a wind speed of 9 m/s reached all sites for at least 1 h. Furthermore, the hours of gust wind > 9 m/s during the day were quantified. When this condition prevailed, a possible dust event day (DED) was assumed. After identifying the dust event days, we proceeded to model numerically 15 selected DEDs, using the criterion of more hours with gust wind. Once the dates of the DEDs to be simulated were obtained, the hourly averages of the previous day (DED-1) allowed identifying the day of the storm for each event. In this way, it was possible to calculate the average behavior (composite) of the 15 events for the two analyzed days.

Additional verification was carried out using Cloud-Aerosol Lidar with Orthogonal Polarization (CALIOP) data (<https://www-calipso.larc.nasa.gov/>). The Cloud-Aerosol Lidar and Infrared Pathfinder Satellite Observation (CALIPSO) satellite provide data on clouds and atmospheric aerosols. CALIPSO combines an active lidar instrument with visible and passive infrared imagers to probe the vertical structure of the atmosphere (Winker et al. 2007). This data helps to identify high-resolution vertical profiles with depolarized measurements for aerosol identification, including the mineral dust fraction (Liu et al. 2008; Liu, Z. et al. 2020). Each one of the 15 DEDs was defined as a true positive when dust was identified in depolarized profiles.

WRF-Chem numerical model

The numerical experiments to simulate dust storms were carried out using the WRF-Chem model version 3.6 (Skamarock et al. 2008; Kumar et al. 2014; Su & Fung, 2015). The WRF-Chem configuration included two domains centered at 22.43°N and 102.65°W (Fig. 1b, also Fig. S1 for modeling detail). The implemented mesh was composed of 120 × 120 grid points of 15-km horizontal resolution and a second inner mesh of 176 × 176 grids of 3-km horizontal resolution, with 29 vertical levels. The model was initialized using the Global Forecast System (GFS) data with 6 h of temporal resolution and 0.5 × 0.5° of horizontal resolution. The parameterizations and dust emission calculations were performed by applying the model configuration used by Kang et al. (2011). The physical settings used in the experiments were the WRF Single-moment 3 Class (WSM3) for microphysics (Hong et al. 2004), the RRTM scheme for longwave radiation (Mlawer et al. 1997), the Dudhia scheme for the shortwave radiation (Dudhia, 1989), the MM5 scheme for the surface layer (Paulson, 1970), Unified Noah for the land-surface model (Tewari et al. 2004), and YSU for the planet boundary layer (Hong et al. 2006). The model calculations of dust emission consider an inert chemical mechanism that contemplates only dust concentration. Several parameterizations are included in the WRF-Chem to estimate the amount of dust emission. In this work, Shao's scheme (2004) was used for the friction velocity threshold, the horizontal sand flux, and the vertical dust flux (Kang et al. 2011; Su & Fung, 2015). Additional data for synoptic charts were generated using the NCEP NARR database of the NOAA/ESRL Physical Science Division, Boulder, Colorado (available at <https://>

psl.noaa.gov/). Composites were calculated for all events using the climatology from 1981 to 2010 (Mesinger et al. 2006).

Soil loss

Dust storms in northern Mexico have arisen due to the intensification of agricultural activity in the region since the 1970s. Intense winds over the ground without vegetation cover, associated with the passage of cold fronts in winter, caused dust storms (Pineda-Martínez et al. 2011; Guevara Macias et al. 2020). In this process, the soil grain size is essential for favoring or inhibiting the dragging process and mineral dust suspension (Wang 2008). The objective is to analyze the soil texture and identify the coarsest fraction, which presents a distribution related to the tillage process in agricultural areas, which are the most affected during dust storms. For this purpose, eight soil samples were collected in previously identified dust emission areas (Guevara Macias et al. 2020) (Fig. S2). An analysis based on remote sensing revealed areas with a significant change in optical properties in the last 30 years. The eight selected sample sites consider the most degraded reported areas. Another objective of soil sampling was to verify the degradation concerning soil erosion by wind intensity and the role of dust emission sources. The sediment sampling occurred during the winter of 2018. The classification of soil samples was done using the size system of the US Department of Agriculture (USDA) (Gee & Or 2002). The samples were separated using seven sieves with the following size openings: 125 μm , 180 μm , 250 μm , 500 μm , 600 μm , 1 mm, and 2 mm. The soil sample results, separated in size, were plotted to determine the soil particle size distribution in the study area. The dust emission scheme in WRF-Chem allows the calculation of the dust emission for each model grid point in terms of land use. This emission data is calculated by the WRF Preprocessing System (WPS) and simulated meteorological fields. Dust in WRF-Chem is

distributed into 5 size bins, calculated intrinsically by the WPS. For the 15 simulated cases, the emission model computes the dust eroded ($\mu\text{g}/\text{m}^2\text{s}$) at each grid point in during the modeling performance. Thus, it is possible to calculate the total dust amount emitted in each event E_i and infer the total accumulated effect in this study period by adding the emissions for all simulated cases, as follows:

$$E_t = F * DE_h \quad (1)$$

where E_t corresponds to total dust emission for dust event day in ton/km^2 , and F is the dust flux emitted as defined by Shao (2004) $F = \sum_{i=1}^l F(d_i)$, with d_i representing the sand particle size. DE_h represents the emission hours for the dust event.

The calculation corresponded to the amount removed by erosion of fine surface material and suspended as PM10 atmospheric particles. Using this average dust storm and assuming nine events per year allowed estimation of the total potential loss of fine fraction in the affected areas for 15 years, i.e., the period of analyzed data.

Results

Soil characterization

Figure 2 displays the soil particle size distribution in percentages. The total samples have a low rate of fine-sized grain and clay fraction ($< 180 \mu\text{m}$), indicating soil loss with minuscule material. Samples 2 and 7 have the highest percentage of fine sizes $< 180 \mu\text{m}$ (42 to 47%) and were collected in bean cultivation plots. The sampling was carried out in the dry season with bare soil before plowing the land. Samples 3, 4, and 5 have a higher proportion of sand ($> 2 \text{ mm}$) (27 to 31%), in contrast to the smaller ratio of tinier dimensions ($< 125 \mu\text{m}$) (5 to 20%). In comparison,

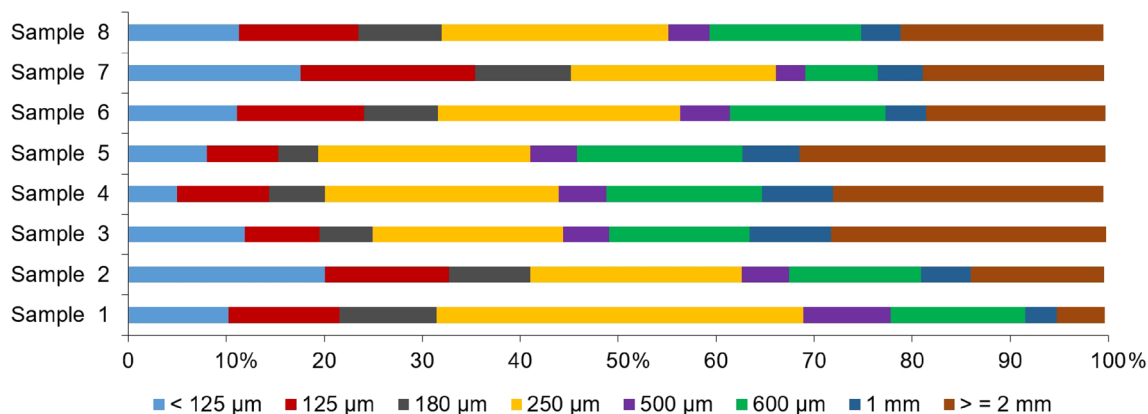


Fig. 2 Particle size from eight soil samples in the study area. The color scale represents the percentage for size distribution

there is a higher percentage in intermediate sizes $< 250 \mu\text{m}$ (20–36%), indicating a size classification of poorly graded sand with silt content (Alfaro & Gomes 2001). The total samples vary in the following form: a low percentage of sizes $< 125 \mu\text{m}$ (5–20%), $< 180 \mu\text{m}$ (19–46%), and sizes $< 500 \mu\text{m}$ (46–78%). The soil texture for the study area was classified as fine silty sands with low clay content (Gee & Or 2002). The samples also show high concentrations of silicates and quartz, as previously reported for this region (Lee et al. 2009; Rivera-Rivera et al. 2010). It is relevant to emphasize that the samples correspond to sites identified as dust emission sources (Pineda-Martinez et al. 2011).

Wind speed analysis

In the study area, the incidence of cold fronts from the north and northwest is a determining phenomenon in the winter season and fundamental in soil erosion. The selected dust storms correspond to the type of events called dry cold fronts of a synoptic nature (Huang et al. 2015). Cold fronts are associated with winds and dust storms from moderate to very intense speed; they can last as long as 1 to 2 days. Figure 3 describes the maximum daily wind speed for 2011 at the 02-AB meteorological station in the study site. The dashed line indicates the 9 m/s value. The peaks present in winter (from September to April) are associated with the passage of cold fronts. There is high variability throughout the year.

Figure 4a shows the eight automatic weather stations with average annual wind speed data. The wind speed varies seasonally, resulting in higher values during the winter (between 4 and 7.5 m/s) (Fig. 4a). The wind direction is predominantly south-southwestern in the winter months. Figure 4b displays the days in which wind speeds exceed 9 m/s.

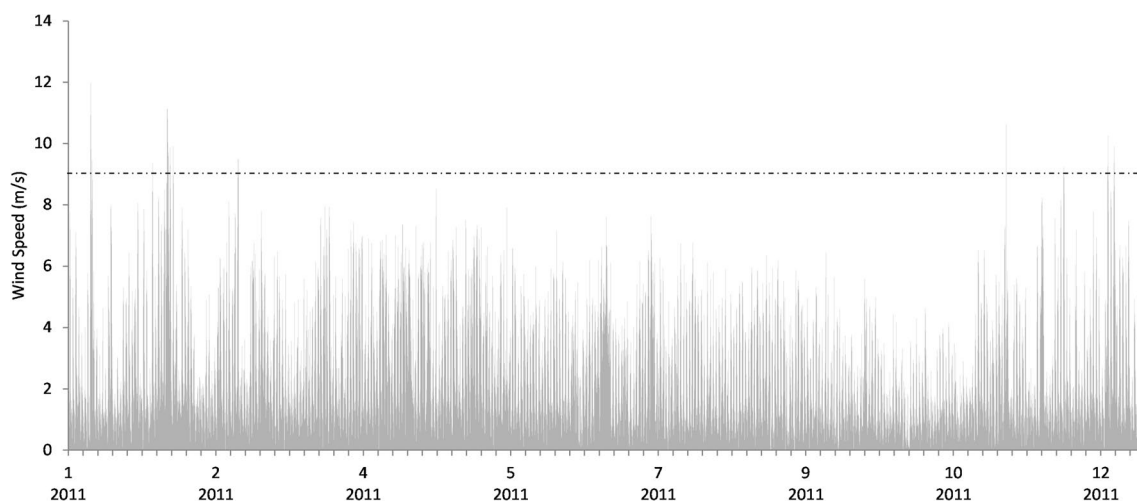


Fig. 3 Maximum daily wind speed throughout 2011 at the Ábrego 02-AB meteorological station located within the study area; discontinuous line indicates the 9 m/s threshold

This speed indicates a high potential for a dust storm event to develop. In Mexico, the National Meteorological Service counted an average of 44 cold front events for the winter season, from September to May, from 2001 to 2016 (SMN 2018). The data analysis from automatic stations yielded 245 cases as potential DED between 2006 and 2018 (the database is available as supplementary material), from which only 15 were chosen to be analyzed in detail and modeled.

Meteorology of cold fronts

Figure 5 shows the prevailing weather conditions in the emission area on the previous day (DED-1) and dust event day. The data corresponds to the Zacatecas International Airport (ZCL), located near the central point of domain 2 (D2). The data analysis provided the hourly average of the 15 DEDs of parameters like sea level pressure (SLP), temperature, wind speed, daily maximum wind speed, and dew point. In all front passage cases, the main characteristic is that the wind intensifies between 12 and 15 h of the DED, presenting the maximum peaks in gusts during those hours. These maximums also coincide with a decrease in SLP and dew point. There is no marked decrease in temperatures at the front entrance until the cold air mass establishes in the area.

Synoptic-scale forcing overview

The synoptic conditions that persist in the winter promote an intensification of wind due to the air masses (fronts) traveling from high latitudes towards the south. Figure 6 shows the synoptic charts for the geopotential height (HGT) at 700 hPa, where a high-pressure zone is a recurring pattern at middle levels in the atmosphere. It indicates a pressure edge

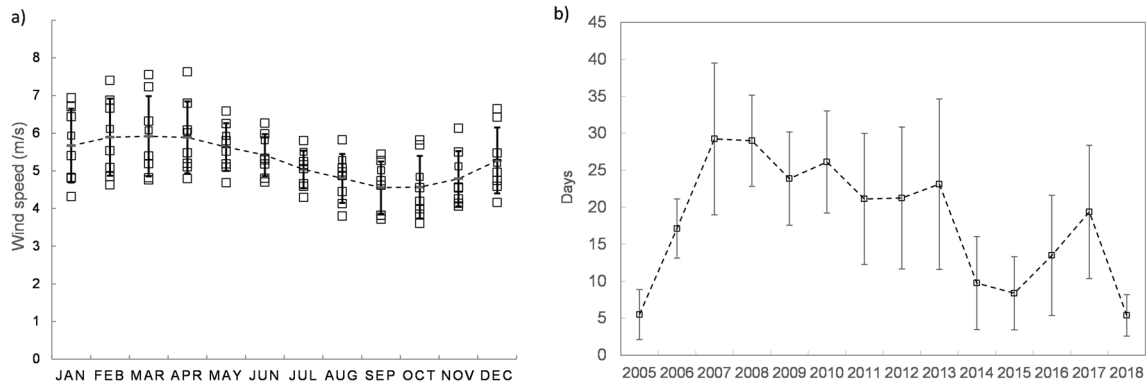


Fig. 4 **a** Monthly averaged wind speed (from 2001 to 2016) for the eight weather stations, and **b** annual number of days exceeding the wind speed threshold (> 9 m/s)

in the cold air mass that drives cold fronts from the USA-MEX border to central Mexico, precisely in the study region, whose entire region is an erodible zone in the Chihuahuan Desert (Rivera-Rivera et al. 2009). This meteorological pattern generates strong winds, dust erosion, and dispersion. The synoptic meteorological conditions are similar, leading to dust event days; for instance, 68% occur within this cold front synoptic environment (Hahnenberger & Nicoll 2012). Some authors have documented the influence of cold fronts in the intensification of winds that generate soil erosion worldwide (Prospero et al. 2002). For example, the impact has been investigated in the Great Basin in the Salt Lake region in Utah (USA) (Hahnenberger & Nicoll 2012; Schultz & Steenburgh 2020), in the New Mexico region, and in northwest Texas in the Dust Bowl region (Lee & Gill 2015; Prospero et al. 2002; Skiles et al. 2018). Other regions like the southwestern USA and northwestern and central Mexico also undergo intense dust storms (Álvarez et al. 2020; Rivera-Rivera et al. 2009; Rivera-Rivera et al. 2010). Wind data analysis in the northern region of Mexico allowed identifying dust storm events based on the maximum velocity criteria for a specific area where this kind of

event has been previously reported in the central highland region (Pineda-Martínez et al. 2011).

The cyclonic dynamics of frontogenesis and propagation is an unstable condition that causes a shift and an intensification of winds (Schultz 2005; Schultz & Steenburgh 2020). Sometimes, wind intensification appears after the front passage, for example, in the Utah region in the USA (Mallia et al. 2017). On the other hand, in low latitudes, wind intensification occurs before the air mass passage (Pineda-Martínez et al. 2011). The front dynamics vary depending on the region and the orientation (Schultz, 2005). Figure 7 shows the composites average distributions of atmospheric pressure (SLP), temperature, and relative humidity obtained from the 15 DEDs. The maximum gradient appears in that transition ahead of the front, which coincides with the high surface erosion (emission). High dust concentrations are mainly associated with increased wind intensity during the passage of cold fronts. This erosion process is a fundamental consequence of the massive change in land use from pasture and forest to agriculture. Besides wind erosion and air quality deterioration, soil decline is also due to open-pit mining activity prevailing in the region.

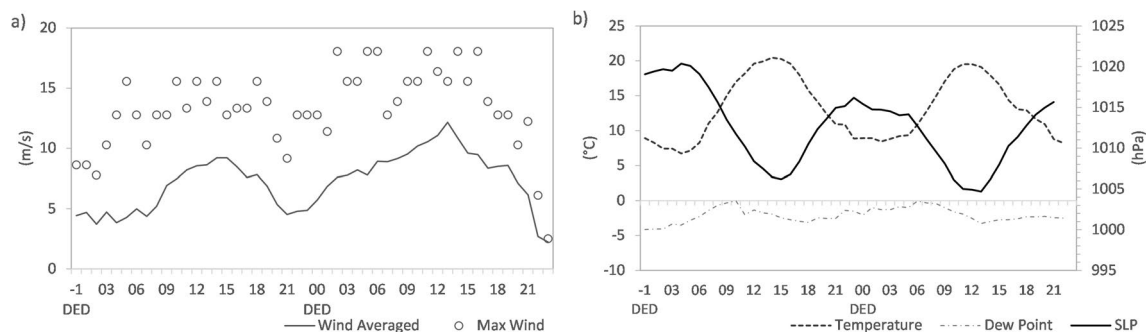


Fig. 5 Hourly data averaged for the 15 DEDs at the center of the domain. **a** Mean and maximum hourly wind speed and **b** sea level pressure (SLP), temperatures, and dew point. The data is also shown for the previous day (− 1 DED).

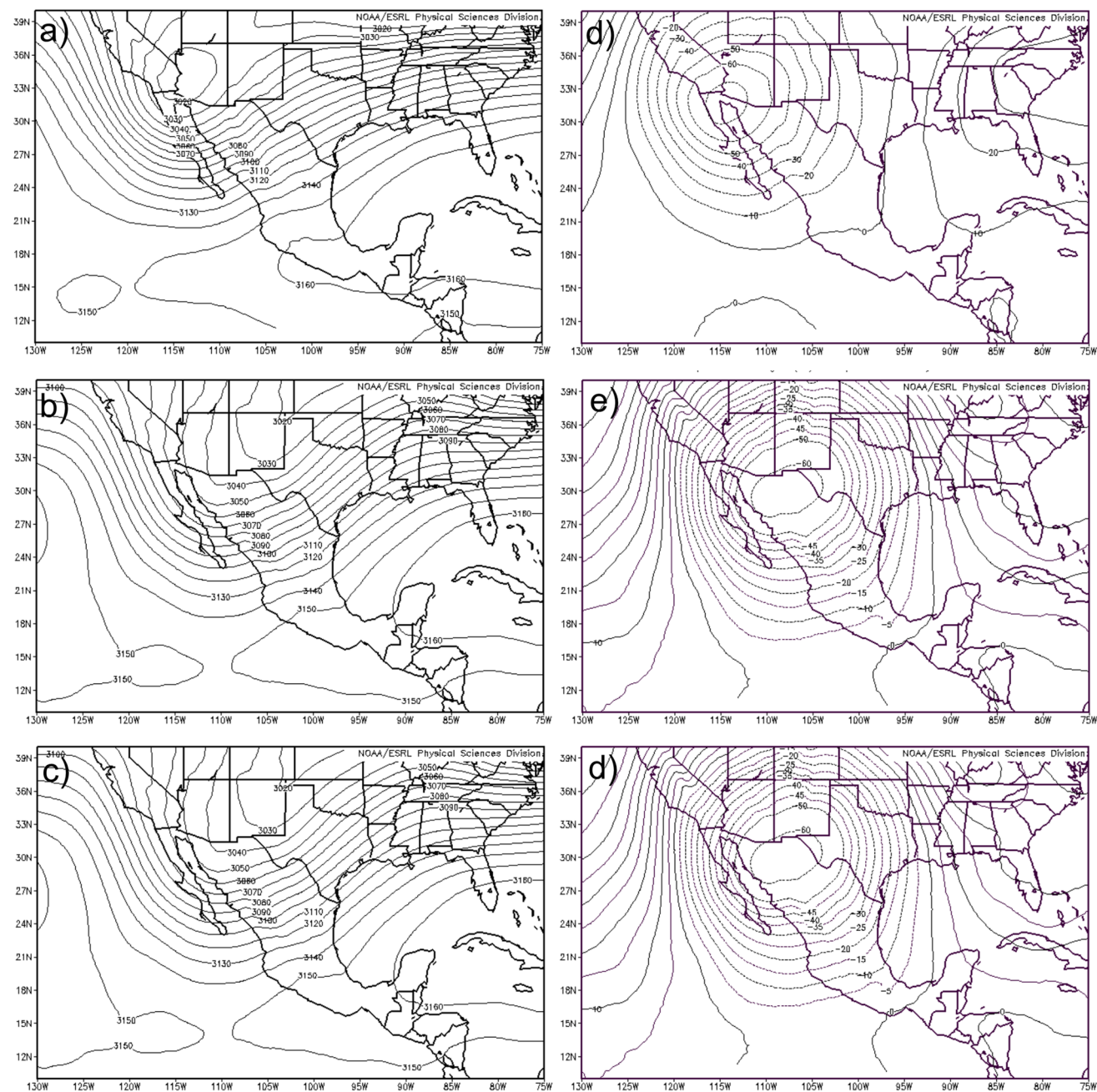


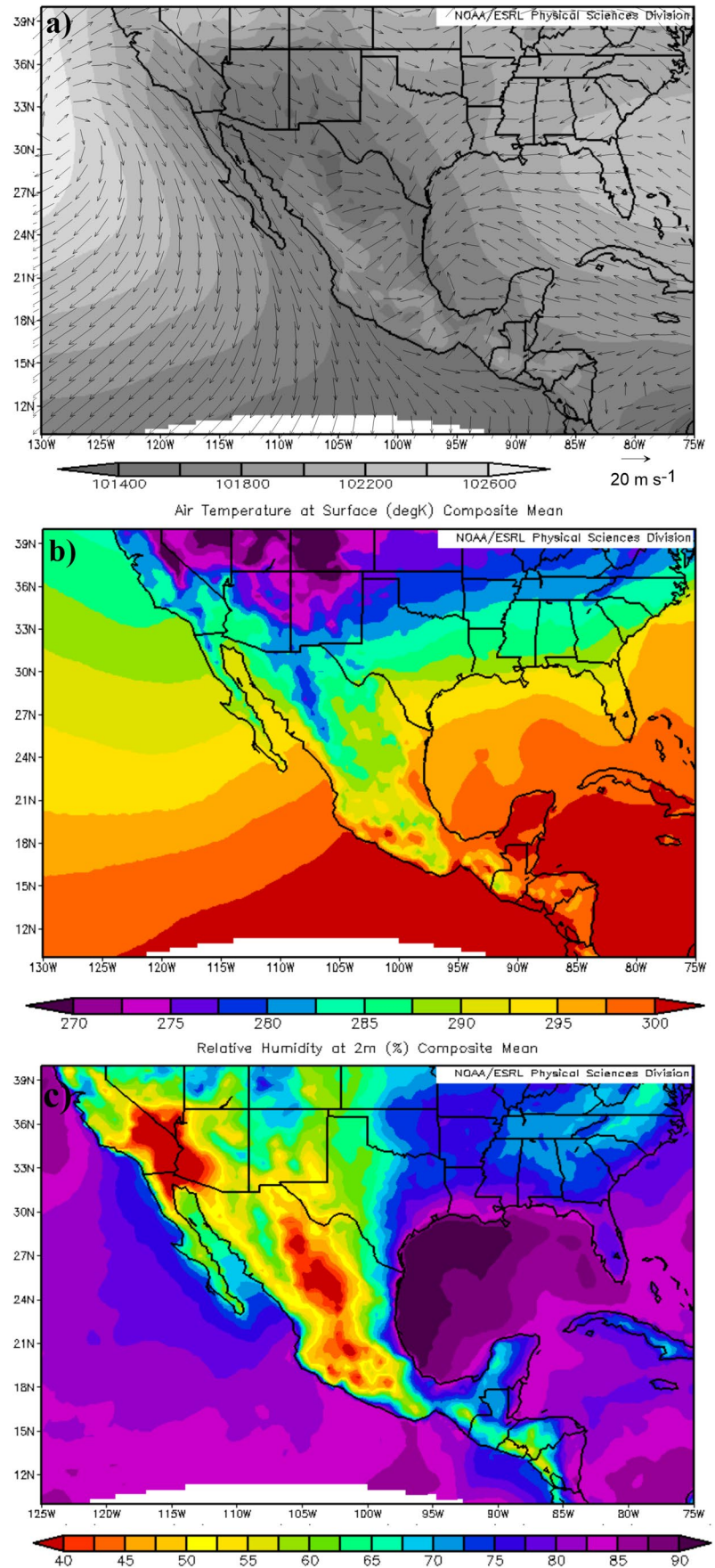
Fig. 6 Composite chart for all dust event days (DED) at 700 mb geopotential height (m) from NCEP/NCAR reanalysis. The left column corresponds to the composite mean for **a** the previous day of the event (-1 DED), **b** for the event date, and **c** the following day ($+1$

1 DED). In the right column are displayed the anomalies for **d** the previous day of the event (-1 DED), **e** for the event date, and **f** the following day ($+1$ DED)

From December to April, even May, wind speed intensifies with the passage of cold air masses as a condition of the geostrophic balance (Schultz & Schumacher 1999; Pineda-Martínez & Carbajal 2009). Months of intense winds are also low or null in rainfall in the Chihuahuan Desert (Choi & Fernando 2008). Both conditions cause a more significant impact on the generation of wind erosion

and, consequently, the degradation of soil (Rivera-Rivera et al. 2009; Lee et al. 2009), but they are also a relevant factor in the emission of particulate matter into the atmosphere as fugitive emissions (Prospero et al. 2002). These emissions deteriorate air quality in cities and small towns, including even more remote regions (Pineda-Martínez et al. 2009; Álvarez & Carbajal 2019).

Fig. 7 Composite of the 15 events just for DED for **a** composite SLP (Pa) and wind vectors ms^{-1} , **b** surface temperature (K), and **c** relative humidity (%)



WRF-Chem simulations

Figure 8 describes the entrance of the cold front to the study area on December 27, 2006. The temperature is significantly lower in the semicircular zone than in the surroundings, and the intensity and wind direction are very different. The wind convergence process and a favorable meteorological synoptic situation notably intensify the wind speed. Therefore, the cold air moving over soil without vegetation cover triggers soil erosion and dust storms. It is also possible to observe how a lower temperature in the incoming cold front causes an increase in relative humidity. During the cold front passage, the temperature is lower than in the southern region of the domain. However, the relative humidity remains in the same order (Fig. 8). This fact reveals that the air mass in the southern area has higher moisture content than the incoming air mass. During the passage of a cold front, general conditions of low relative humidity (< 40 %), a decrease in temperature (< 5 °C), and an intensification of the wind speed (> 10 m/s) prevail. Figure 8 displays the temperature distribution associated with the air mass and the wind's intensification defining a preferential southwest-northeast direction. In the simulated December 2006 event, the cold air mass intrusion into the region can be observed. All the cases display a similar pattern in terms of temperature and humidity. However, temperatures and relative humidity values varied from case to case but had similar orders of magnitude. It is also interesting to note that the wind vectors always align in a similar direction, and their intensification coincides with the region of flat topography in the Mexican highlands. Thus, this region is a source of mineral dust particles and fugitive emissions, representing meteorological conditions that cause negative effects on human health by a high concentration of PM10 near urban sites.

Table 1 summarizes the values of each event simulated by applying the WRF-Chem model. All events correspond

to the 2006–2018 period between December and April during the maximum cold front activity. The highest concentration values correspond to the events between February and April when high wind speed and low relative humidity persist. The wind speed data also indicates that events are more intense in certain years. Consequently, the values of PM10 increased in April 2009 and February 2011. North America also had one of the most critical droughts in similar conditions (Seager et al. 2014). In contrast, the years with lower concentrations (2006 and 2017) showed a decrease in the average wind speed.

Dust storm modeling

The impact of dust storms is considerable, causing massive soil deterioration and health problems due to excessively elevated PM10 concentrations, according to the daily Mexican Official Standard of $70 \mu\text{g}/\text{m}^3$ (NOM, 2021). Based on the average maximum concentration of PM10, each event was grouped into four intensity categories: weak, medium, high, and extreme (Fig. 9). The classification must be completed due to the complexity of the erosion process. Several factors include the specific incidence of the wind (direction and speed) on the agricultural land areas with high soil loss potential, for instance, the pre-existing soil moisture, and the environmental conditions that determine the dust storm in this semi-arid region.

Figure 9 displays each particular event feature, revealing defined patterns of the sources, dust transportation, and concentrations of PM10. Most cases were in group IV (low), with a maximum concentration of $34 \mu\text{g}/\text{m}^3$. In group III, the medium intensity was between 60 and $120 \mu\text{g}/\text{m}^3$. The high-intensity group II had an average concentration between 50 and $150 \mu\text{g}/\text{m}^3$, above the Mexican Standard ($70 \mu\text{g}/\text{m}^3$, an average of 24 h). On February 3, 2011, the only extreme case in group I had a concentration value of more than $350 \mu\text{g}/\text{m}^3$.

Fig. 8 Simulation of the entrance of a cold front to the study area (domain D2). **a** Temperature and wind at 22:30 UTC and **b** relative humidity at 14:30 UTC, both on December 27, 2006

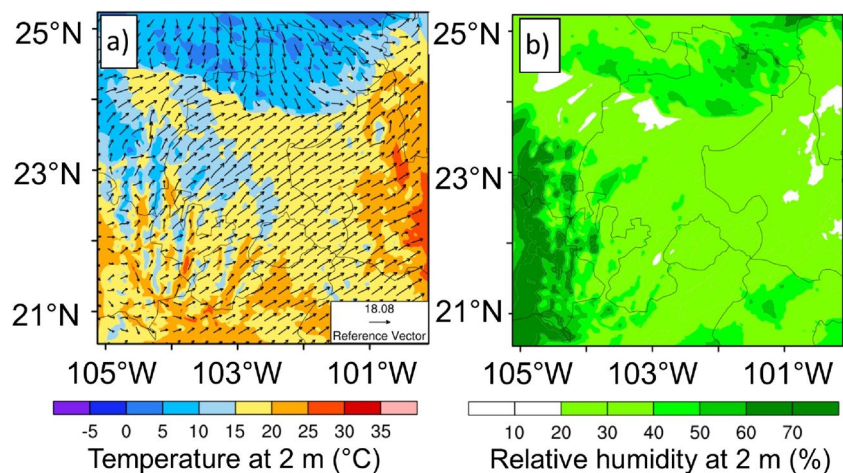


Table 1 The data summarize a comparison of observed and simulated dust events by applying the WRF-Chem model. The data corresponds to the central point of domain 1 (D2) in WRF-Chem and the Zacatecas International Airport (ZCL) meteorological station observation data. Temperature and relative humidity (RH %) at 2-m level are the 24-h averages for the dust event day. Wind represents the maximum value reached during the DED. Statistical metrics for model validation were performed in IBM SPSS Statistics (Version 21)

Date of DED	Temperature (°C)		RH (%)		Max Wind (m/s)	
	WRF	ZCL	WRF	ZCL	WRF	ZCL
Dec 29, 2006	5.00	9.90	40.80	43.50	15.80	15.60
Jan 31, 2007	10.30	9.50	59.60	55.30	18.20	12.80
Feb 14, 2007	12.00	13.90	26.50	24.50	14.30	13.90
Feb 16, 2008	13.90	13.90	30.70	25.80	12.30	12.80
Apr 11, 2009	16.90	18.60	25.10	21.80	17.00	15.60
Dec 01, 2009	9.10	10.50	53.90	68.00	19.70	18.10
Mar 09, 2010	11.60	15.10	24.60	43.00	17.40	15.60
Feb 3, 2011	9.90	12.60	64.10	40.90	17.80	17.50
Mar 20, 2012	11.80	14.30	32.70	32.50	12.50	14.40
Feb 21, 2013	12.40	15.20	39.20	30.30	12.40	15.60
Dec 27, 2015	10.10	12.00	48.60	48.70	17.90	18.10
Mar 9, 2016	10.50	7.10	49.00	55.70	18.20	18.10
Feb 13, 2017	14.10	17.10	30.60	25.80	10.90	12.80
Dec 7, 2017	9.10	15.10	46.50	40.00	12.20	18.10
Apr 10, 2018	16.20	17.90	38.80	26.30	30.80	18.10
<i>RMSE</i>		2.942		9.953		4.091
<i>r</i> ²		0.746*		0.709*		0.519*
<i>BIAS</i>		1.048		− 0.236		2.613

*Significant correlations at confidence level of 95%

m³. This case occurred during an extraordinary drought that impacted much of Mexico and the southern USA (Seager et al. 2014).

The emission and transport of dust vary regarding the emission source points. It is a more complicated issue to define their characteristics a priori due to the landscape heterogeneity. However, it had a similar dispersion pattern in all simulated events, i.e., SW-NE dust storm orientation coincides with the dominant and intense winter winds. Another characteristic of storm events is duration and persistence, between 1 and 2 days. In DEDs of higher wind speed, the transport of dust particles will reach a more considerable distance. For groups I and II, dust storms generated in central Mexico arrive north of Texas in the USA (Pineda-Martinez et al. 2011). Seasonal wind patterns also have high interannual variability. It indicates that the emission of dust will be extreme for some years. For instance, the most intense dust storm occurred on February 3, 2011. Figure 9a reveals that the concentrations reached values of 520 µg/m³.

In the extreme event (case I), a considerable emission range reaches an extension of more than 100 km and is displaced to the east. In adjacent areas, the emission values are of the order of 160 µg/m³. Wind rates reached more than 9 m/s, and the total dust emission varied between 1.2 tons and 937 tons in the 15 selected DEDs. As previously mentioned, not all intense wind speeds generate dust storms; other factors, such as soil moisture content and relative humidity, are influential.

In urban zones close to the study area, air quality data reported during the winter periods exceeded the Mexican Standards in maximum values of 24 h for several days. During the years 2006, 2007, and 2008, in cities such as Torreon (210 µg/m³), Durango (180 µg/m³), and Zacatecas (200 µg/m³), average monthly values surpassed the Mexican Standards between November and March (SEMARNAT, 2018). All these values negatively affect health in urban areas and cause respiratory diseases in central and northern Mexico (Cabrera-Cano et al. 2021).

Model validation using CALIPSO observations

Because it was impossible to perform a numerical validation of the observed data of PM10 on the surface, verification of the simulated output was carried out by using the CALIOP Level 1B data, which contains calibrated and geo-referred single-shot lidar profiles. This approach to detecting and monitoring sand and dust storms has been applied in various regions, including the southwestern USA (Vukovic et al. 2014).

Since the surface tracks of CALIPSO profiles do not always pass over the study area for the day of the event, it was necessary to include various orbit tracks to validate the event. In the 15 selected events, atmospheric dust was corroborated during the simulated day. For all cases, we used data from the daytime and nighttime tracks. Given the nature of dust storms associated with cold fronts, it is feasible to observe the emission and presence of dust for more than 1 day and in at least one track, where the belt of intense winds

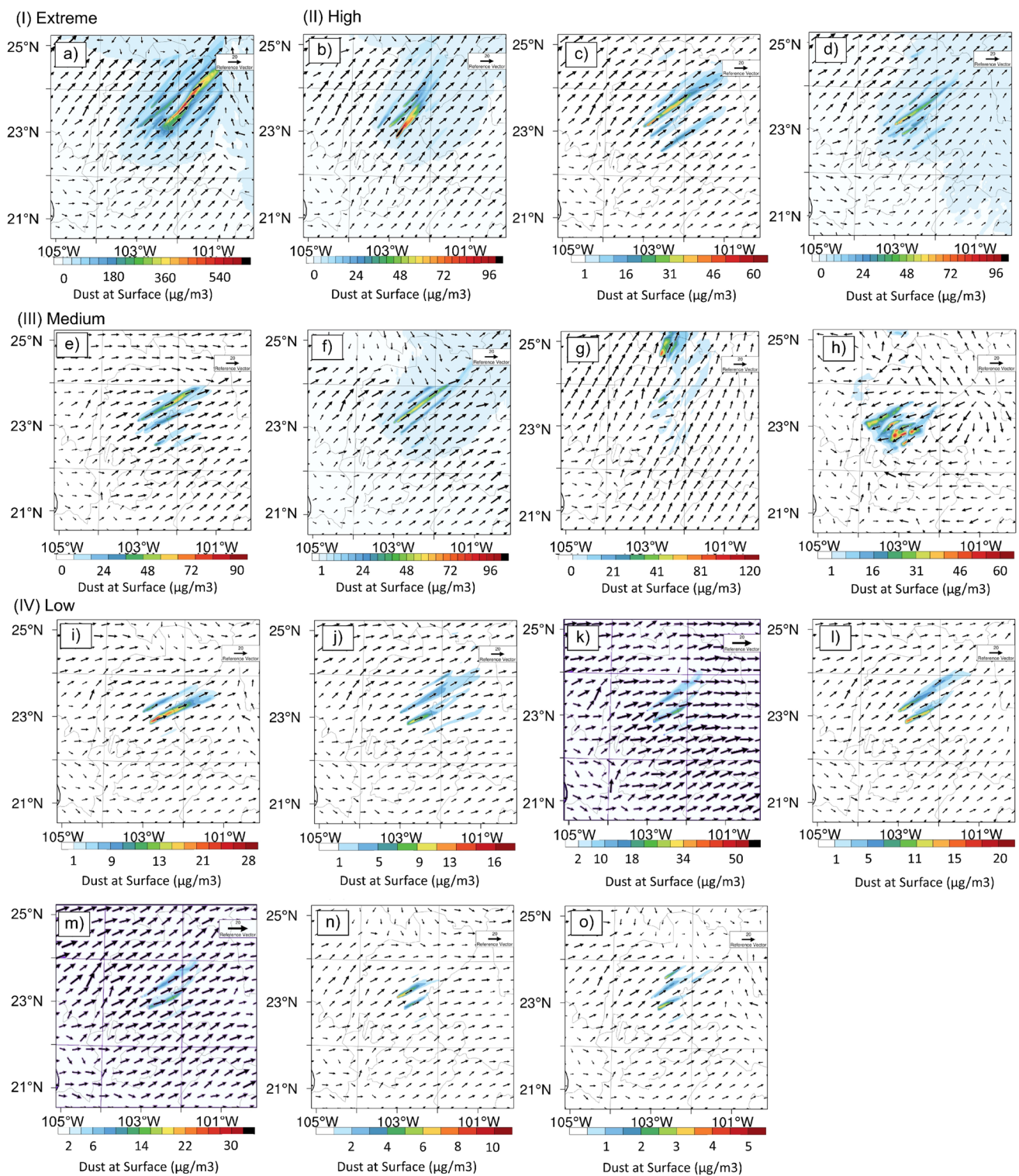


Fig. 9 WRF-Chem data from dust storm events groups in D2. **a** Group I represents the extreme case of February 3, 2011. Group II of high intensity: **b** December 29, 2006, **c** January 31, 2007, and **d** April 11, 2009. Group III of medium intensity: **e** December 1, 2009,

f December 27, 2015, **g** March 8, 2016, and **h** April 10, 2018. Group IV of low intensity: **i** February 14, 2007, **j** February 16, 2008, **k** March 10, 2010, **l** March 20, 2012, **m** February 21, 2013, **n** February 14, 2017, and **o** December 7, 2017

advances with the displacement of the air mass (Schultz 2005). From the CALIPSO profiles, the dust intensity can be anticipated, such as for the numerical simulations. In some profiles, extensive distribution of dust was found, showing a high contribution of PM₁₀ that affects the air quality in that area, in addition to indirectly observing the height at which they are dispersed (Fig. 10).

In recent decades, the study region has experienced a rapid land use change, mainly from grassland and shrublands to rainfed agriculture (Guevara Macias et al. 2020). It is relevant to point out that agriculture in the semi-arid region takes place in areas with scarce water sources and severe soil degradation. It has been observed in dust storm events in Texas that agricultural soils are more prone to erosion even than desert soils, hence the importance of conducting a study on the erosive processes that occur in this area (Chen & Fryrear 2002). In the study region, the rainfall is low during the winter, and the vegetation cover is minimal. Consequently, much of the soil undergoes repeated erosion due to strong winds associated with the passage of cold fronts. Wind speed analysis revealed that the wind records exceed the speed threshold of 9 m/s for erosion or dust removal in up to 20 events per year in meteorological stations located in the region. However, it is required to have better assurance about the formation of a dust storm. Periods of moderate

to intense drought are frequent phenomena in northern Mexico and the southern USA. Previous studies on this phenomenon indicate that at least four moderate to extreme drought events occurred during our study period, with 2011 being the most intense and prolonged (Seager et al. 2014; Vega-Camarena et al. 2018).

The next step was to assess the study region's erosive potential for dust storms. Calculating the emission rates for each grid point of the domain and the 15 modeled dust storms allowed estimating the total dust eroded. The total loss of the fine fraction (PM₁₀) indicates the deterioration of soils in the study region (Fig. 11). This calculation shows the potential for soil loss due to wind effects, which overlaps with previous estimations (Echavarría et al. 2009). The calculation of potential soil loss is very relevant to estimate soil degradation. In recent decades there has been a massive change from the use of land with vegetation cover to land for agricultural use with rainfed irrigation (Guevara Macias et al. 2020). Often these soils are exposed to intense winds with the respective erosion processes. In addition, dust storms generated in these areas deteriorate air quality in large urban areas. It fully justifies the importance of estimating soil erosion. The methodology presented in this research work can be improved with greater availability of data on wind, ground cover, and knowledge of dust particle sizes.

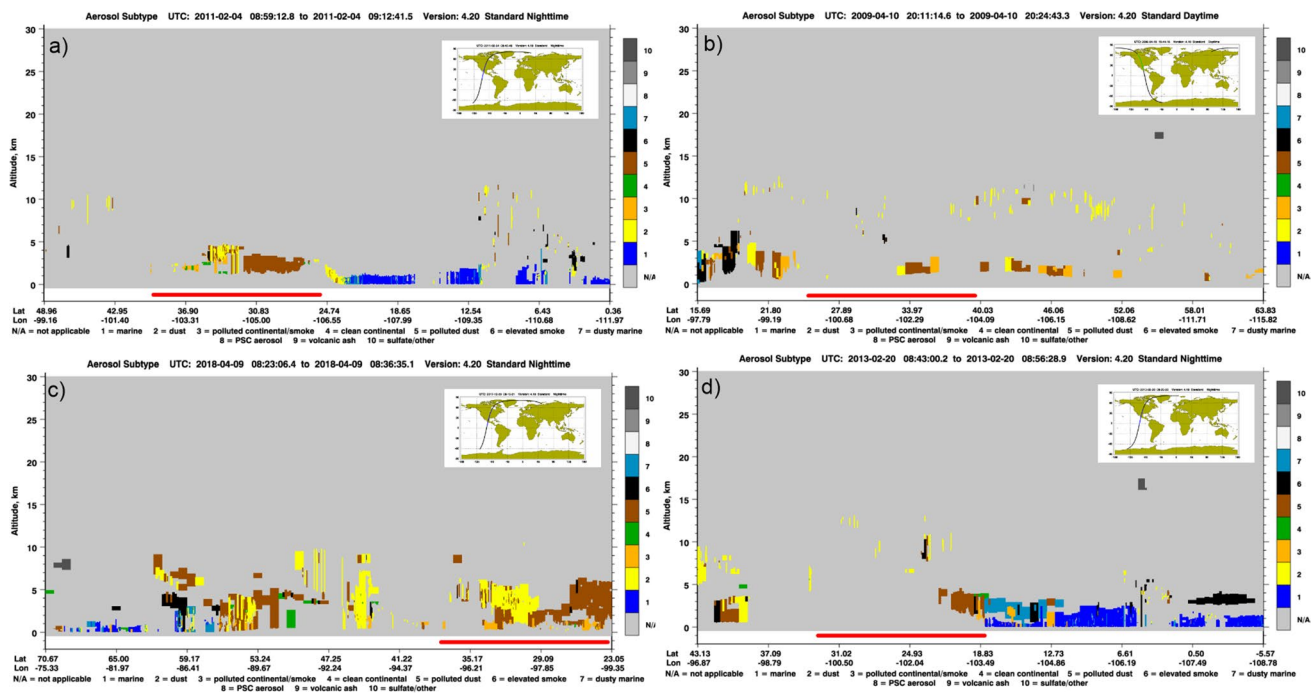
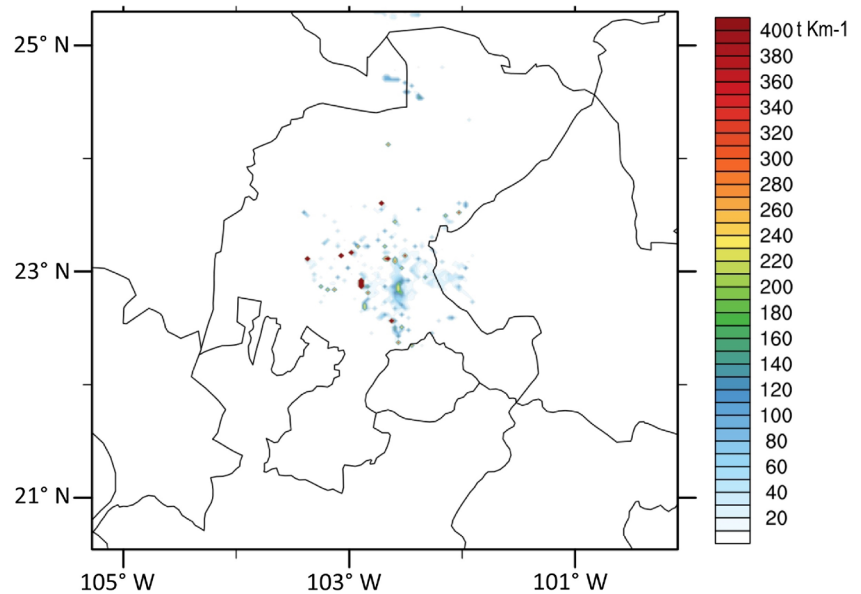


Fig. 10 Satellite profiles of dust storm events showing the CALIPSO aerosol subtype for **a** nighttime passage of 2011 Feb. 04 (at 08:59 to 09:12 UTC), **b** daytime of 2009 Apr. 10 (at 20:53 to 21:06 UTC), **c** nighttime of 2018 Apr. 09, and **d** nighttime of 2013 Feb. 20. The red

line at the bottom indicates the location of the study area during the satellite track. The CALIPSO overpass is shown on the interior maps of each plot

Fig. 11 Estimation of total potential soil loss for the 15 dust storm events in D2. The areas correspond to the WRF-Chem model grids considered as dust sources



Factors affecting PM10 simulations

The limitations when using a numerical model for simulating dust storms depend on many factors, which have been discussed previously by Hyde et al. (2018, and references therein). These factors can be separated into two large groups: those associated with the data on the properties of the surface and the sources of dust emission and the factors associated with the event. First, a dynamic update of the soil cover is required, as well as a constant characterization of the soil particles that are susceptible to being eroded by the action of the wind. The soil properties will determine the wind speed thresholds for dust emission (Hyde et al. 2018). Second, the characteristics associated with dust storm events must be considered (Pineda-Martinez et al. 2011; Huang et al. 2015; Hyde 2018); their intensity depends on the wind, the soil moisture conditions, and the presence of precipitation in previous days, among others. During each event, it is also essential to observe the intensity of the wind gusts and the duration in effective hours of the gusts of intense wind, which will determine the maximum PM10 concentration peaks. Although the numerical model can become a valuable tool in forecasting and managing air quality issues associated with dust dispersion, it requires much information to improve its calibration and adaptation to specific local conditions. Increasing spatial and temporal resolution of the monitoring data for the quantitative validation would be an important subject for completing the qualitative analyses based on the satellite and radar data. This work tries to present a preliminary exercise of modeling the phenomenon of dust storms to point out that it is a problem paltry studied in the northern region of Mexico.

Conclusions

In north-central Mexico, dust storms associated with intense winds were identified during the passage of cold fronts. Each dust storm event causes an increase in the concentrations of PM10 above those established by Mexican Standards. Beyond being a semi-desert area, the change in land use to agricultural areas causes a decrease in plant structure, causing an intensification of erosion events and emission of atmospheric dust. There is a high interannual behavior associated with this seasonal wind pattern, indicating that dust emissions could reach extreme conditions in certain years. The analysis of wind data in the study period showed that there are a high number of days that exceed the wind speed threshold with the possibility for the generation of dust storms each year in northern Mexico. Of these identified dust storm cases, 15 were selected for modeling. The CALIPSO data was an option to validate each of the 15 simulated cases. Nevertheless, many more dust emission events may occur considering the intensification of the winds in the north of Mexico during the winter. WRF-Chem data shows that atmospheric dust concentrations during dust storms exceeded Mexican Standards. The methodology proposed in this work can help future investigations regarding this environmental problem in semi-arid areas.

Supplementary Information The online version contains supplementary material available at <https://doi.org/10.1007/s11869-023-01365-6>.

Author contribution Conceptualization, Noel Carbajal and Luis F Pineda-Martinez; numerical modeling, Maria de Jesus Guevara. Data analysis and validation, F Pineda-Martinez and Maria de Jesus Guevara. All the authors drafted the manuscript and contributed to discussion of the results.

Funding This study was partially supported by CONACYT with a research grant of Maria de Jesus Guevara Macias (230709).

Data availability The datasets generated during the current study are available from the corresponding author request.

Declarations

Ethics approval and consent to participate All procedures performed in this study were following the ethical standards of the institutional and/or national research committee. All the authors agree to participate in this research.

Consent for publication The authors declare that they agree with the publication of this paper in this journal.

Conflict of interest The authors declare no competing interests.

References

- Alfaro SC, Gomes L (2001) Modeling mineral aerosol production by wind erosion: emission intensities and aerosol size distributions in source areas. *J Geophys Res-Atmos* 106-16:18075–18084. <https://doi.org/10.1029/2000JD900339>
- Álvarez CA, Carbajal N (2019) Regions of influence and environmental effects of Santa Ana wind event. *Air Qual Atmos Health* 12:1019–1034. <https://doi.org/10.1007/s11869-019-00719-3>
- Álvarez CA, Carbajal N, Pineda-Martínez LF, Tuxpan J, Flores DE (2020) Dust deposition on the Gulf of California caused by Santa Ana winds. *Atmosphere* 11(3):275. <https://doi.org/10.3390/atmos11030275>
- Barnett AG, Fraser JF, Munck L (2012) The effects of the 2009 dust storm on emergency admissions to a hospital in Brisbane. *Australia Int J Biometeorol* 56:719–726
- Basha G, Phanikumar DV, Kumar KN, Ouarda TB, Marpu PR (2015) Investigation of aerosol optical, physical, and radiative characteristics of a severe dust storm observed over UAE. *Remote Sens Environ* 169:404–417
- Cabrera-Cano AA, Cruz-de la Cruz JC, Gloria-Alvarado AB, Álamo-Hernández U, Riojas-Rodríguez H (2021) Asociación entre mortalidad y covid-19 y contaminación atmosférica en ciudades mexicanas. *Salud Publica Mex* 63(4):470–477
- Chen W, Fryrear DW (2002) Sedimentary characteristics of a haboob dust storm. *Atmos Res* 61(1):75–85
- Choi YJ, Fernando HJS (2008) Implementation of a windblown dust parameterization into MODELS-3/CMAQ: application to episodic PM events in the US/Mexico border. *Atmos Environ* 42:6039–6046. <https://doi.org/10.1016/j.atmosenv.2008.03.038>
- Csavina J, Field J, Felix O, Corral-Avitia AY, Eduardo-Sáez A, Berton EA (2014) Effect of wind speed and relative humidity on atmospheric dust concentrations in semi-arid climates. *Sci Total Environ* 487:82–90. <https://doi.org/10.1016/j.scitotenv.2014.03.138>
- Dong Z, Wang X, Liu L (2000) Wind erosion in semiarid China: an overview. *J Soil Water Conserv* 55:439–444
- Dudhia J (1989) Numerical study of convection observed during the winter monsoon experiment using a mesoscale two-dimensional model. *J Atmos Sci* 46(20):3077–3107. [https://doi.org/10.1175/1520-0469\(1989\)046<3077:NSOCOD>2.0.CO;2](https://doi.org/10.1175/1520-0469(1989)046<3077:NSOCOD>2.0.CO;2)
- Echavarría CFG, Medina-García G, Rumayor-Rodríguez AF, Serna-Pérez A, Salinas-González H, Bustamante-Wilson JG (2009) Diagnóstico de los recursos naturales para la planeación de la intervención tecnológica y el ordenamiento ecológico. INIFAP, CIRNOC, Campo Experimental Zacatecas Libro Técnico Núm 10:174
- Foley JA, DeFries R, Gregory A, Barford C, Gordon B, Carpenter SR, Chapin FS, Coe MT, Daily GC, Gibss HK, Helkowski JH, Holloway T, Howard EA, Kucharik CJ, Monfreda C, Patz JA, Prentice C, Ramakutty N, Snyder PK (2005) Global consequences of land use. *Science* 309:570–574. <https://doi.org/10.1126/science.1111772>
- Gee GW, Or D (2002) Particle-size analysis. In: Dane JH, Topp GC (eds) *Methods of soil analysis. Part. 4. Physical methods*. SSSA Book Ser. 5. SSSA, Madison, pp 255–293
- Grineski SE, Staniswalis JG, Bulathsinhala P, Peng Y, Gill TE (2011) Hospital admissions for asthma and acute bronchitis in El Paso, Texas: do age, sex, and insurance status modify the effects of dust and low wind events? *Environ Res* 111(8):1148–1155. <https://doi.org/10.1016/j.envres.2011.06.007>
- Guevara Macías MJ, Carbajal N, Tuxpan-Vargas J (2020) Soil deterioration in the southern Chihuahuan Desert caused by agricultural practices and meteorological events. *J Arid Environ* 176:104097. <https://doi.org/10.1016/j.jaridenv.2019.104097>
- Hahnenberg M, Nicoll K (2012) Meteorological characteristics of dust storm events in the eastern Great Basin of Utah, U.S.A. *Atmos Environ*:601–612. <https://doi.org/10.1016/j.atmosenv.2012.06.029>
- Holben BN, Eck TF, Slutsker IA, Tanre D, Buis JP, Setzer A, Vermote E, Reagan JA, Kaufman YJ, Nakajima T, Lavenu F, Jankowiak I, Smirnov A (1998) AERONET—a federated instrument network and data archive for aerosol characterization. *Remote Sens Environ* 66(1):1–16. [https://doi.org/10.1016/S0034-4257\(98\)00031-5](https://doi.org/10.1016/S0034-4257(98)00031-5)
- Hong SY, Dudhia J, Chen SH (2004) A revised approach to ice microphysical processes for the bulk parameterization of clouds and precipitation. *Mon Weather Rev* 132(1):103–120
- Hong SY, Noh Y, Dudhia J (2006) A new vertical diffusion package with an explicit treatment of entrainment processes. *Mon Weather Rev* 134(9):2318–2341
- Huang M, Tong D, Lee P, Pan L, Tang Y, Stajner I, Pierce R, McQueen J, Wang J (2015) Toward enhanced capability for detecting and predicting dust vents in the western United States: the Arizona case study. *Atmos Chem Phys* 15:12565–12610. <https://doi.org/10.5194/acp-15-12595-2015>
- Hyde P, Mahalov A, Li J (2018) Simulating the meteorology and PM10 concentrations in Arizona dust storms using the Weather Research and Forecasting model with Chemistry (Wrf-Chem). *J Air Waste Manage Assoc* 68(3):177–195
- INEGI (2015) Carta de uso de suelo y vegetación. Datos vectoriales. Escala 1 250 000 serie V
- Instituto Nacional de Investigaciones Forestales Agrícolas y Pecuarias INIFAP (2018) Red de Monitoreo Agroclimático del Estado de Zacatecas. Retrieved from: <http://www.zacatecas.inifap.gob.mx>. Accessed 22 Sept 2022
- Joshi JR (2021) Quantifying the impact of cropland wind erosion on air quality: a high-resolution modeling case study of an Arizona dust storm. *Atmos Environ* 263:118658. <https://doi.org/10.1016/j.atmosenv.2021.118658>
- Kang JY, Yoon SC, Shao Y, Kim SW (2011) Comparison of vertical dust flux by implementing three dust emission schemes in WRF/Chem. *J Geophys Res-Atmos* 116D9. <https://doi.org/10.1029/2010JD014649>
- Karegar E, Hossein Hamzeh N, Bodagh Jamali J, Ranjbar Saadat Abadi A, Moeinaddini M, Goshtasb H (2019) Numerical simulation of extreme dust storms in east of Iran by the WRF-Chem model. *Nat Hazards* 99(2):769–796. <https://doi.org/10.1007/s11069-019-03773-3>
- Kok J, Ridley D, Zhou Q et al (2017) Smaller desert dust cooling effect estimated from analysis of dust size and abundance. *Nat Geosci* 10:274–278. <https://doi.org/10.1038/ngeo2912>
- Kumar R, Barth MC, Pfister GG, Naja M, Brousseau GP (2014) WRF-Chem simulations of typical pre-monsoon dust storm in northern

- India: influences on aerosol optical properties and radiation budget. *Atmos Chem Phys* 14:2431–2446. <https://doi.org/10.5194/acp-14-2431-2014>
- Lambin EF, Geist HJ, Lepers E (2003) Dynamics of land-use and land-cover change in tropical regions. *Annual Rev Env Resour* 28(1):205–241. <https://doi.org/10.1146/annurev.energy.28.050302.105459>
- Lee JA, Gill TE (2015) Multiple causes of wind erosion in the Dust Bowl. *Aeolian Res* 16–36. <https://doi.org/10.1016/j.aeolia.2015.09.002>
- Lee JA, Gill TE, Mulligan KR, Dominguez-Acosta M, Pérez AE (2009) Land use/land cover and point sources of the 15 December 2003 dust storm in southwestern North America. *Geomorphology* 105.1–2.18–27. <https://doi.org/10.1016/j.geomorph.2007.12.016>
- Liu YF, Liu Y, Shi ZH, López-Vicente M, Wu GL (2020) Effectiveness of re-vegetated forest and grassland on soil erosion control in the semi-arid Loess Plateau, CATENA. 195:104787. <https://doi.org/10.1016/j.catena.2020.104787>
- Liu Z, Liu D, Huang J, Vaughan M, Uno I, Sugimoto N, Kittaka C, Trepte C, Wang Z, Hostetler C, Winker D (2008) Airborne dust distributions over the Tibetan Plateau and surrounding areas derived from the first year of CALIPSO lidar observations. *Atmos Chem Phys* 8:5045–5060. <https://doi.org/10.5194/acp-8-5045-2008>
- Lu D, Fitzgerald R, Stockwell WR, Reddy RS, White L (2013) Numerical simulation for a wind dust event in the US/Mexico border region. *Air Qual Atmos Hlth* 62:317–331. <https://doi.org/10.1007/s11869-012-0174-7>
- Mallia DV, Kochanski A, Wu D, Pennell C, Oswald W, Lin JC (2017) Wind-blown dust modeling using a backward-Lagrangian particle dispersion model. *J Appl Meteorol Climatol* 56:2845–2867. <https://doi.org/10.1175/JAMC-D-16-0351.1>
- Mesinger F, DiMego G, Kalnay E, Mitchell K, Shafran PC, Ebisuzaki W, Jovic D, Woollen J, Rogers E, Berbery EH, Ek MB, Fan Y, Grumbine R, Higgins W, Li H, Lin Y, Manikin G, Parrish D, Shi W (2006) North American regional reanalysis: a long-term, consistent, high-resolution climate dataset for the North American domain, as a major improvement upon the earlier global reanalysis datasets in both resolution and accuracy. *Bull Am Meteorol Soc* 87:343–360. <https://doi.org/10.1175/BAMS-87-3-343>
- Middleton NJ (2017) Desert dust hazards: a global review. *Aeolian Res* 24:53–53
- Mlawer EJ, Taubman SJ, Brown PD, Iacono MJ, Clough SA (1997) Radiative transfer for inhomogeneous atmospheres: RRTM, a validated correlated-k model for the longwave. *J Geophys Res Atmos* 102:16663–16682. <https://doi.org/10.1029/97JD00237>
- Munson SM, Belnap J, Okin GS (2011) Responses of wind erosion to climate-induced vegetation changes on the Colorado Plateau. *PNAS*. 108(10):3854–3859. <https://doi.org/10.1073/pnas.1014947108>
- Norma Oficial Mexicana NOM (2021). NOM-025-SSA1-202. Criterio para evaluar la calidad del aire ambiente, con respecto a las partículas suspendidas PM10 y PM2.5
- Paulson CA (1970) The mathematical representation of wind speed and temperature profiles in the unstable atmospheric surface layer. *J Appl Meteorol* 9:857–861. [https://doi.org/10.1175/1520-0450\(1970\)009<0857:TMROWS>2.0.CO;2](https://doi.org/10.1175/1520-0450(1970)009<0857:TMROWS>2.0.CO;2)
- Pineda-Martínez LF, Carbajal N (2009) Mesoscale numerical modeling of meteorological events in a strong topographic gradient in the northeastern part of Mexico. *Clim Dyn* 332–3:297–312. <https://doi.org/10.1007/s00382-009-0549-0>
- Pineda-Martínez LF, Carbajal N, Campos-Ramos AA, Noyola-Medrano C, Aragón-Piña A (2011) Numerical research of extreme wind-induced dust transport in a semi-arid human-impacted region of Mexico. *Atmos Environ* 45:4652–4660. <https://doi.org/10.1016/j.atmosenv.2011.05.056>
- Prospero JM, Ginoux P, Torres O, Nicholson SE, Gill TE (2002) Environmental characterization of global sources of atmospheric soil dust identified with the Nimbus 7 Total Ozone Mapping Spectrometer (TOMS) absorbing aerosol product. *Rev Geophys* 40(1):1002. <https://doi.org/10.1029/2000RG000095>
- Rezaei M, Sameni A, Shamsi SRF, Bartholomeus H (2016) Remote sensing of land use/cover changes and its effect on wind erosion potential in southern Iran. *PeerJ* 4:e1948. <https://doi.org/10.7717/peerj.1948>
- Rivera-Rivera NI, Gill TE, Bleiweiss MP, Hand JL (2010) Source characteristics of hazardous Chihuahuan Desert dust outbreaks. *Atmos Environ* 44:2457–2468. <https://doi.org/10.1016/j.atmosenv.2010.03.019>
- Rivera-Rivera NI, Gill TE, Gebhart KA, Hand JL, Bleiweiss MP, Fitzgerald RM (2009) Wind modeling of Chihuahuan Desert dust outbreaks. *Atmos Environ* 43:347e354. <https://doi.org/10.1016/j.atmosenv.2008.09.069>
- Schultz DM (2005) A review of cold fronts with prefrontal troughs and wind shifts. *Mon Weather Rev* 133:2449–2472. <https://doi.org/10.1175/MWR2987.1>
- Schultz DM, Schumacher PN (1999) The use and misuse of conditional symmetric instability. *Mon Weather Rev* 127:2709–2732. <https://doi.org/10.1175/1520-04931999127<2709:TUAMOC>2.0.CO;2>
- Schultz DM, Steenburgh WJ (2020) Nonclassic evolution of a cold-frontal system across the Western United States during the Intermountain Precipitation Experiment IPEX. *Wea Forecasting* 35:255–271. <https://doi.org/10.1175/WAF-D-19-0166.1>
- Schweitzer MD, Calzadilla AS, Salamoá O, Sharife A, Kumard N, Holta G, Campos M, Mirsaedia M (2018) Lung health in era of climate change and dust storms. *Environ Res* 163:36–42
- Seager R, Goddard L, Nakamura J, Henderson N, Lee DE (2014) Dynamical causes of the 2010/11 Texas–northern Mexico drought. *J Hydro-meteorol* 15(1):39–68. <https://doi.org/10.1175/JHM-D-13-024.1>
- SEMARNAT (Secretaría de Medio Ambiente y Recursos Naturales) (2018) Programa para Mejorar la Calidad del Aire en la Región de la Comarca Lagunera 2010–2015. Retrieved from: <http://www.semarnat.gob.mx/>. Accessed 3 Oct 2022
- Shao Y (2004) Simplification of a dust emission scheme and comparison with data. *J Geophys Res* 109:1–6. <https://doi.org/10.1029/2003JD004372>
- Skamarock WC, Klemp JB, Dudhia J, Gill DO, Barker DM, Wang W and Powers JG (2008) A description of the Advanced Research WRF version 3. NCAR Technical note-475+ STR
- Skiles SM, Flanner M, Cook JM, Dumont M, Painter TH (2018) Radiative forcing by light729 absorbing particles in snow. *Nat Clim Chang* 8:964–971. <https://doi.org/10.1038/s41558-730018-0296-5>
- SMN (Servicio Meteorológico Nacional) (2018) Cold fronts climatology 2001–2016. Retrieved from: <https://smn.conagua.gob.mx/es/climatologia/pronostico-climatico/frentes-frios>. Accessed 29 Sept 2022
- Su L, Fung JC (2015) Sensitivities of WRF-Chem to dust emission schemes and land surface properties in simulating dust cycles during springtime over East Asia. *J Geophys Res Atmos* 120(11):215–11,230. <https://doi.org/10.1002/2015JD023446>
- Tewari M, Chen F, Wang W, Dudhia J, LeMone MA, Mitchell K, Ek M, Gayno J, Wegiel J, Cuenca RH (2004). Implementation and verification of the unified NOAA land surface model in the WRF model. In 20th conference on weather analysis and forecasting/16th conference on numerical weather prediction (1115, 6, pp. 2165–2170).
- Vega-Camarena JP, Brito-Castillo L, Farfán LM, Gochis DJ, Pineda-Martínez LF, Díaz SC (2018) Ocean–atmosphere conditions related to severe and persistent droughts in the Mexican Altiplano. *Int J Climatol* 38(2):853–866. <https://doi.org/10.1002/joc.5215>

- Vukovic A, Vujadinovic M, Pejanovic G, Andric J, Kumjian MR, Djurdjevic V, Sprigg WA (2014) Numerical simulation of “an American haboob”. *Atmos Chem Phys* 14(7):3211–3230
- Wang X, Dong Z, Zhang J, Liu L (2004) Modern dust storms in China: an overview. *J Arid Environ* 58:559–574. <https://doi.org/10.1016/j.jaridenv.2003.11.009>
- Wang X, Xia D, Wang T, Xue X, Li J (2008) Dust sources in arid and semiarid China and southern Mongolia: impacts of geomorphological setting and surface materials. *Geomorphology* 97(3–4):583–600. <https://doi.org/10.1016/j.geomorph.2007.09.006>
- Winker DM, Hunt WH, McGill MJ (2007) Initial performance assessment of CALIOP. *Geophys Res Lett* 34:L19803. <https://doi.org/10.1029/2007GL030135>
- Zhao C, Liu X, Leung LR (2012) Impact of the desert dust on the summer monsoon system over Southwestern North America. *Atmos Chem Phys* 12:3717–3731. <https://doi.org/10.5194/acp-12-3717-2012>

Publisher’s note Springer Nature remains neutral with regard to jurisdictional claims in published maps and institutional affiliations.

Springer Nature or its licensor (e.g. a society or other partner) holds exclusive rights to this article under a publishing agreement with the author(s) or other rightsholder(s); author self-archiving of the accepted manuscript version of this article is solely governed by the terms of such publishing agreement and applicable law.